Magnetic Data for Delineating Subsurface Structures and Estimating Magnetic Sources Depth of Magnetic Intrusive in Farigh Area, Sirt Basin

Ahmed.S.Saheel *, Abdul Rahim Bin Samsudin ** and Umar Bin Hamzah **

Abstract: The studied area is characterized by having complex structures that trend mainly in the NW–SE, and E–W directions. Magnetic data is used to delineate the subsurface structures and to estimate the magnetic sources depth of the selected area in Farigh area, Sirt basin Libya. Power spectrum analysis, Horizontal gradient technique, Analytic Signal and 3D Euler deconvolution technique using standard deviation filters have been applied in order to achieve the above mentioned goals. Interpretation of the onshore magnetic anomaly of this area, suggests that the high total magnetization may be caused by an intrusive body. Analysis of the magnetic power spectra indicates the presence of four sub-anomalies at depths of 350 m, 1400 m, and 2525 m which probably related to the igneous rocks. The presence of igneous rock as basement at depth of 4740 m was confirmed by drilling J1-12. Assuming that all rock magnetization in the area is caused by induction in the present geomagnetic field, it strongly suggests that the causative structure has a remnant magnetization of declination D= 2.322^{o} and inclination (*I)* = 41.579^{o}. Based on magnetic data, the total Horizontal derivative map shows high gradient values in E-W trends related to the structures in the eastern part of the Sirte basin. An analytic signal method was applied to the aeromagnetic data to estimate locations and the minimum depths to the contact. The depth values for profiles 1,2,3,4,5 respectively 1400m,1430m, 2744m,2190m and 1415m. The depth from well J1-12 is 1400m matched to the depth results from profile 5 (1415m). The 3D Euler deconvolution map derived from magnetic data clearly indicates the location of igneous body in the study area as well as its tectonic trends and depth, which is estimated at 350 m to 1400 m below the surface. Depth of magnetic anomalies at 1400 m to 2525 m is considered as anomalies in between shallow and deep. Anomaly at depth of approximately 4740 m below the surface is interpreted as basement rock. Geologically, the magnetic survey shows that the source of anomaly is a mafic igneous rock of Early Cretaceous in age. The study also discovered a left-lateral sheared fault zone along the NW-SE of Hercynian in age which was believed to be reactivated during Early Cretaceous.

Keywords: Magnetic data, Igneous bodies, Power spectrum analysis, Horizontal gradient technique, Analytic Signal and 3D Euler deconvolution.

INTRODUCTION

The study area which is about 114 km^2 is located in the southern part of Concession 12 of Veba Oil field (Fig. 1). This report presents the results of processing and analysis of aeromagnetic field data over the southern part of the Farigh Low. The aeromagnetic survey data was acquired between February and May 2006 by Worley Parsons GPX Pty. Ltd. The survey area was between 21^{o} 05 ˙and 21^{0} 20’ East, and between 28^{0} 42’ and 28^{0} 57’ North. The survey had a traverse spacing of 500m (azimuth, 45º & 225^{o}) and a tie line spacing of 2.5km (azimuth, 135º & 315^{o}). The nominal terrain clearance of the survey aircraft was 137m. The magnetic data was supplied by the acquisition contractor in UTM zone 34N (Hayford1924) coordinates. This was the coordinate system used for all interpretation. The final High Resolution Aero Magnetic (HRAM) data was supplied in grids of 300x300m. The inclination and declination of the centre of the survey area were 41.579^{o} and 2.322^{o} respectively.

The principal aim of this study was to determine the depth and extent of the extrusive volcanic rocks within or overlying the Nubian Sandstone.

*Libyan Petroleum Institute-Tripoli-Libya, P.O.Box 6431
**School of Environment and Natural Resource Sciences, Faculty of Science and Technology, Universiti Kebangsaan Malaysia, 43600 Bangi, Selangor

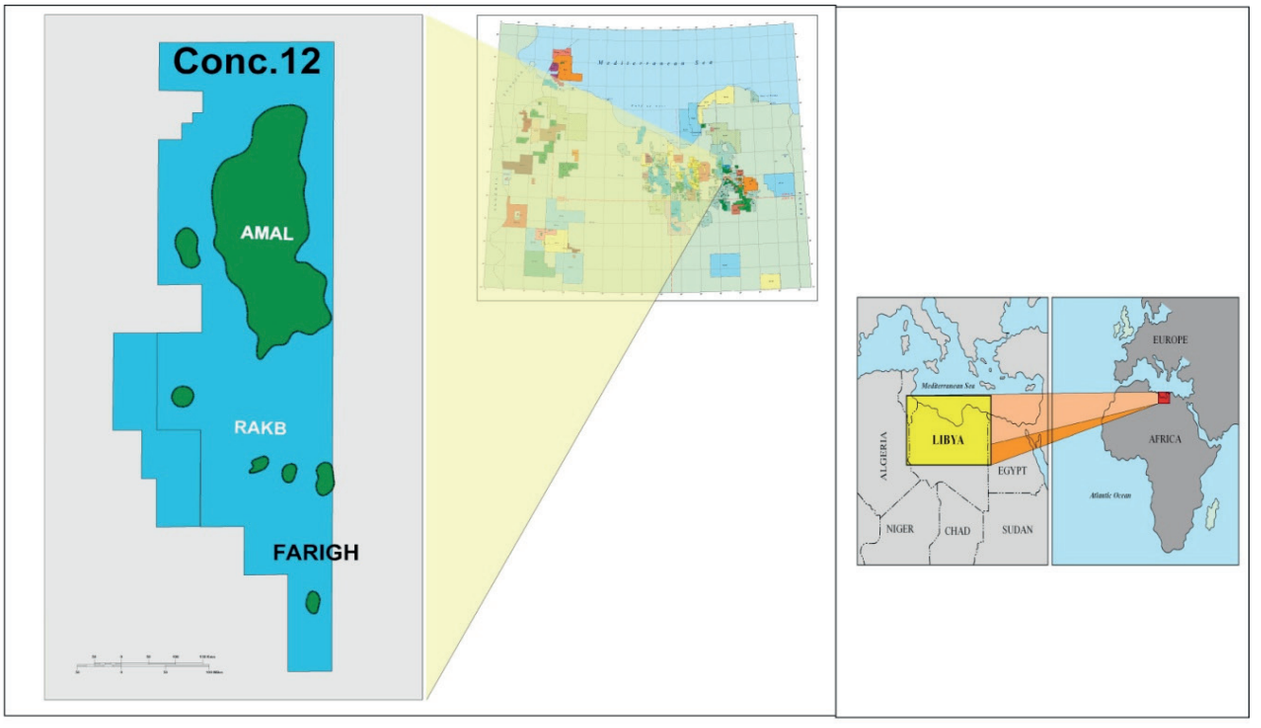

Fig. 1. Location map of the concession 12 in the Sirt basin.

Depth of the volcanic rocks was determined by using the Power spectrum analysis, Horizontal gradient technique, Analytic Signal and 3D Euler deconvolution techniques applied on magnetic data. The Horizontal gradient technique was used to locate boundaries of magnetic data. The final results revealed new information on dominant trends of the lineaments, nature of the intrusive igneous bodies, structural features, and the age of volcanic activity.

GEOLOGICAL SETTING

Farigh is located near the southern boundary of Concession 12 in the eastern part of Sirt Basin. The shallow to intermediate (2 to 3 km depth) sedimentary succession of the Sirt Basin was studied through hundreds of wells data and was divided into three major sequences (Fig. 2). In the central part of the Basin, the succession consists of a pre-rift (pre-Upper Cretaceous) sequence directly overlying the Precambrian basement, and overlain by the syn-rift (Upper Cretaceous-Upper Eocene) and the post-rift (Oligo-Miocene) sequences (Ahlbrandt, 2001). These two sequences were marine in origin and were subdivided into various rock units, but the stratigraphic order and sedimentary characteristics of the post-rift sequence and early pre-rift sequence in the deeper parts of the Basin were poorly

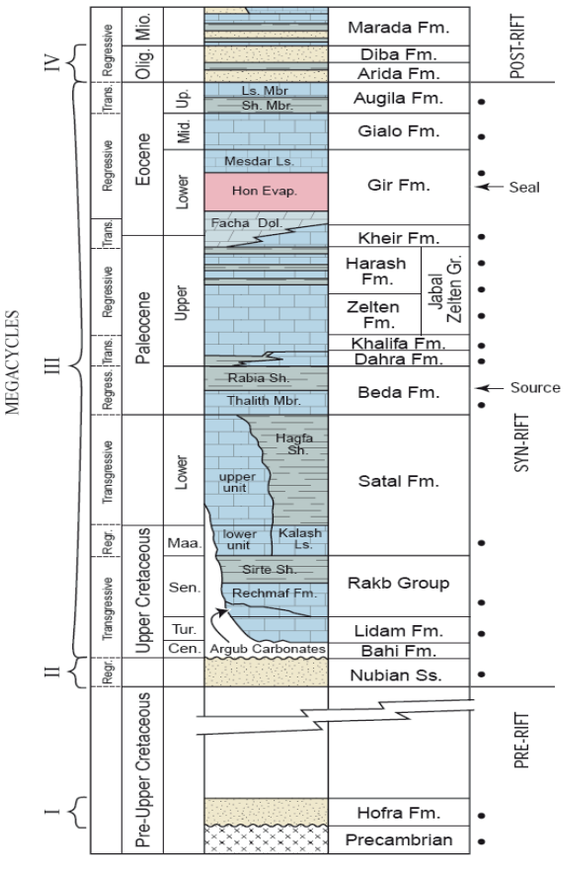

Fig. 2. Stratigraphy section of the Sirt Basin.

understood. The pre-rift (and early-rift) sequence consist of various types of continental siliciclastics deposits with some shallow marine intercalations, as well as volcanics or intrusives, ranging from Lower Paleozoic (in the case of the Gargaf Group) to Late Jurassic- Early Cretaceous (for the Nubian Sandstone and its correlatives). In the eastern part of the Sirt Basin, another sequence of siliciclastics (the Amal Group) was distinguished and entirely assigned as Triassic (Gras and Thusu, 1998). The Nubian Sandstone is best known in Egypt and Sudan, where extensive outcrops were found exposed (Klitzsch and Squyres, 1990). In the eastern part of Sirt Basin (the Sarir Arm), the Nubian was considered to be of late Jurassic to early Cretaceous in age (El-Hawat *et al* 1996) and correlated with the Sarir Sandstone (Gras and Thusu, 1998). In the Farigh area, the Nubian has been penetrated by several wells, having a maximum thickness of 2111 feet (635m), but it has not been drilled through completely. The sequence was divided into five lithological units, often with gradational contacts. All of the units did not occur in the same well. Unit 1, the youngest and often eroded and Unit 4 (131-138m) thick as drilled through at three sites contain intervals of hematitic siltstone or claystone, while all of the units contained one or more layers of pink to brown sandstones and/or white quartzite (Tawadros *et al* 2001). These lithological characteristics are reminiscent of the Triassic "Red Beds", and may have a relatively high magnetic susceptibility compared with typical sandstone due to a high iron oxide content. This may complicate the task of isolating the magnetic signature of intrusives or volcanics within the Nubian, particularly if they have limited lateral continuity, or occur close to the crystalline basement.

***Structure of the Farigh area*:** The major tectonic trends of the Arch were also believed to have controlled the post-Hercynian structure of the Sirt Basin. The Sirt Basin is widely consider to be a failed, tripartite, intra-plate rift (Ahlbrandt, 2001) that started to develop in the Triassic, undergoing multiple-phased rifting, which culminated in the late Cretaceous, followed by post-rift subsidence that ceased in Oligocene. However, in the deepest, northern parts of the Basin, such as the coastal parts of the Ajdabiya Trough, subsidence continues and the thickness of the post-Hercynian sediments may reach up to 8 km (Hallet, 2002). In general, compressional structures are rare, but diastrophic events (uplift, subsidence, tilting, faulting and intrusions) are prevalent (Goudarzi, 1980). The first phase of rifting was considered to have began in the eastern (Sarir) arm of the basin (Hameimat Trough area), culminating in the Neocomian-Barremian with a predominantly E-W orientation. The second phase of mainly NW-SE oriented rifting started within the central part of the Basin in the late Aptian (Fig. 3), migrating towards the north-northwest (Guiraud and Bosworth, 1997). Rifting was accompanied by volcanic activities (van der Meer and Cloetingh, 1993) and followed by thermal subsidence, which was shortly interrupted by inversion in the Santonian, at the peak of the Alpine orogeny (Guiraud and Bosworth, 1997). The Farigh Low is bounded to the north by large listric normal faults, which delineate the boundary between the Farigh Low and the Rakb High, and indicate the opening of the Farigh Low during Early Cretaceous time. The east-west trend of the bounding fault may be indicative of a possible earlier Hercynian faulting stage during Upper Paleozoic time.

***Hydrocarbon history in the study area*:** Drilling for oil exploration began in 1959 and after an initial dry hole, oil was discovered in basal quartzitic sandstones on the northern part of the concession 12 (Roberts 1970, see Fig. 4). The A1-12 well was drilled to a depth of 10,146 feet in the central area of the concession and penetrated a Tertiary-Cretaceous section, overlying a granitic basement with oil shows. The B1-12 well was drilled 34 km north of the first well and encountered a similar uphole section, but penetrated 600 feet of oil bearing quartzitic sandstone without reaching basement granite. Approximately 160 oil wells were drilled in the Amal B, E and N pools and the Amal Field has produced 992 million barrels of oil (February 2005) from the Amal and Maragh sandstones. The Rakb High, identified by the A1-12 well covers the central portion of the concession. The basal sandstones were neither deposited nor removed by erosion. However, reserves have been established on the Rakb High in shallower Eocene reservoirs. For the South of the Rakb High, early drilling established that the Gialo High extended onto southern part of Concession 12 and that a prospective basal sandstone trend was present between the Gialo and Rakb Highs. The Farigh Field was discovered in 1969 when the A1-12 well penetrated a thick oil column in the Nubian sandstone. The field was initially mapped as an isolated structural closure, north of the Gialo High,

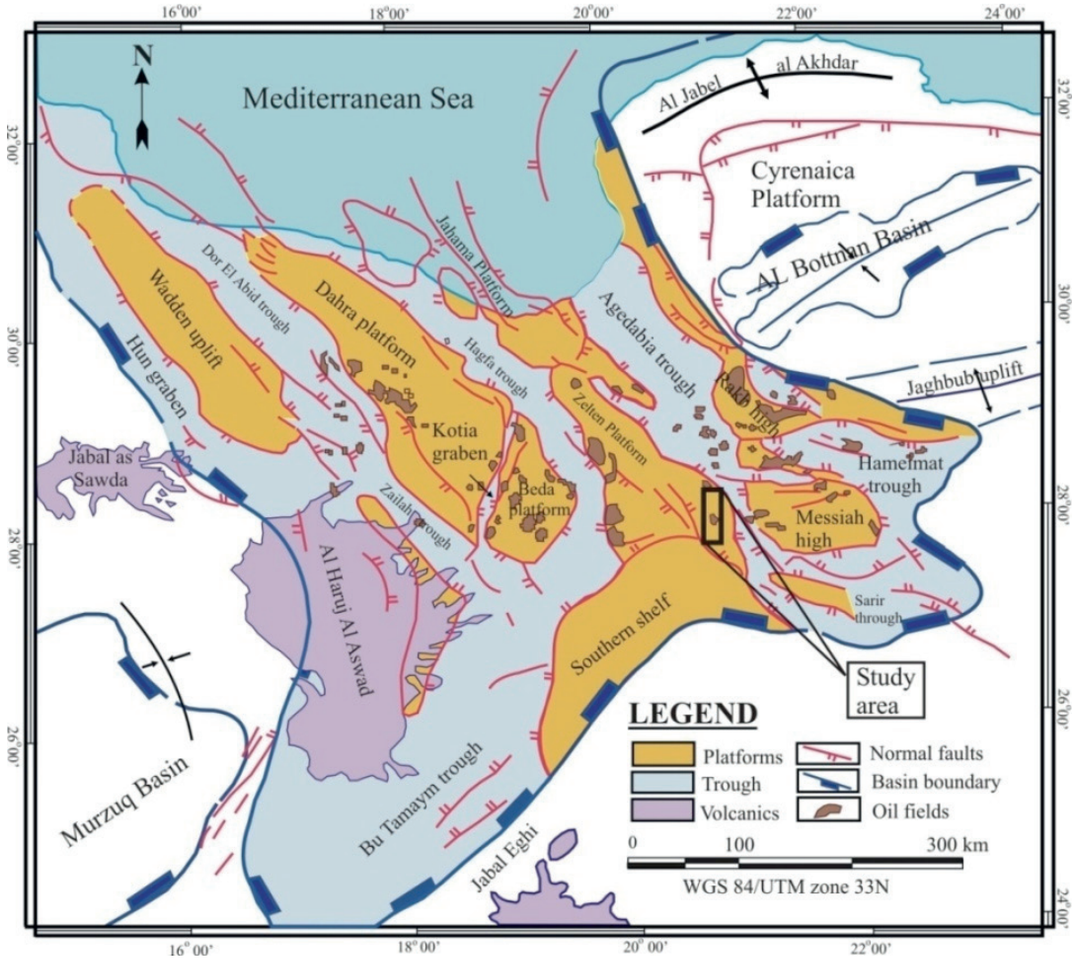

Fig. 3. Tectonic element in the Sirt Basin, (Modified after Abadi, 2002).

and extensive 2-D seismic was shot to evaluate the Concession 12 area south of the Rakb High. The most recent documented geological analysis of the Farigh area (Robertson 1970) concluded that excellent hydrocarbon potential existed in the Farigh U Lead, immediately south of the Farigh Field, and in the Farigh V Lead, 7 km north of the Farigh Field.

GEOPHYSICAL DATA

***Total Magnetic Intensity (TMI)*:** The total magnetic intensity map (TMI) of the Farigh area was calculated in an attempt to delineate its subsurface structure (Fig. 5). Majority of the Farigh area is characterized by positive magnetic anomalies. This area was clearly represented as a minimum magnetic closure (42029 to 42073 nT), and the dominant trend within the study area was NW-SE. The minimum values occurring in the north and west of the area (42030 to 42080 nT) indicate thick sediment. The high positive magnetic anomalies reflected in the eastern and southern part (42088-42161 nT) indicated the presence of highly magnetic material. This can be interpreted as an anticline structure defining the existence of outcrops of Oligocene-Miocene rocks (the oldest unit in the area) on the surface. The magnetic data showed the presence of intrusive igneous bodies in the southern part of the study area trending E-W in direction.

The magnetic data were processed and transformed into Power spectrum, Total horizontal gradient, analytic Signal and 3D Euler deconvolution (Figs. 6, 7, 8, & 9). These data contained many high frequency anomalies originated from cultural sources such as power lines, pipelines and oil wells. The Geosoft software was used to transform the Poisson equation relating the gravity and magnetic field potentials expressed by $U = -(J/G\rho)\ (\partial V/\partial I)$, where U, V, I, J, ρ and G were, respectively, magnetic potential, gravitational potential, direction of magnetization, magnetization intensity, density and Gravitational constant (Geosoft, 2009).

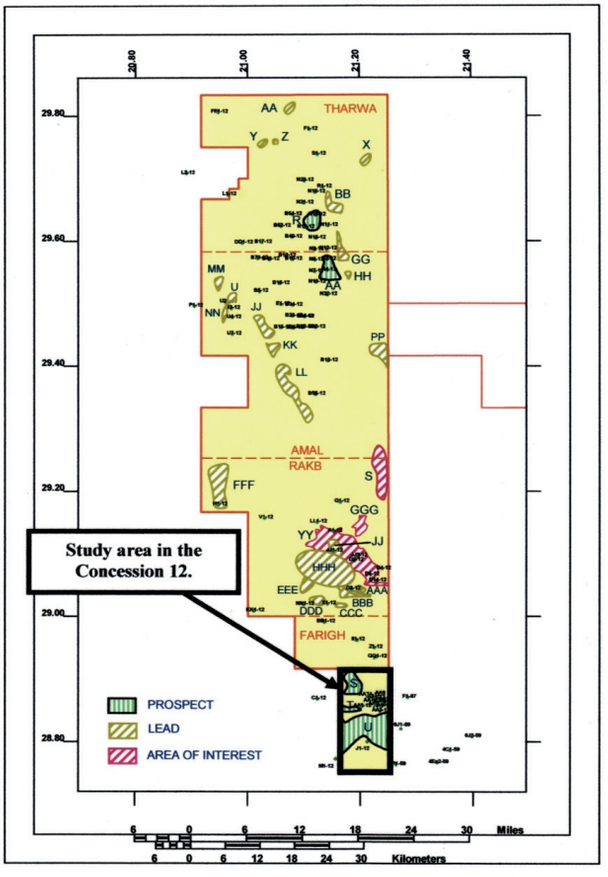

Fig. 4. Location map showing the hydrocarbon potential areas

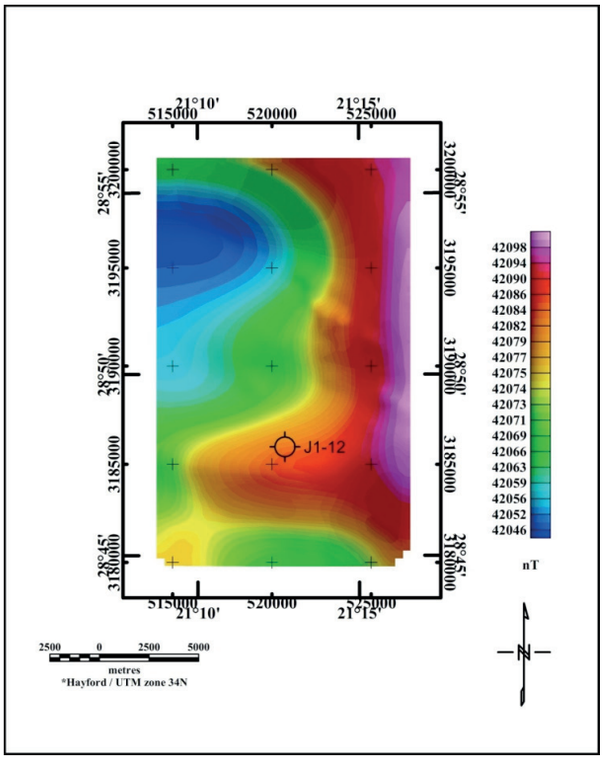

Fig. 5. Total Magnetic Intensity (TMI) map of Farigh area, using grid cell size 400m.

***Power spectrum analysis*:** The power spectrum of the reduced to the pole magnetic grid, which represented the magnitude of various frequency components of a 2D image, was computed by Fourier transform and seems in agreement with the location of the main source at the origin of the anomaly (Geosoft, 2009). The spectrum shows 4 very clear anomalies at depths below aircraft of 350m, 1400m, 2525m and 4740m. The shallowest slice (Fig. 6) at depth 350m appeared to correspond very strongly to surface features A interpreted as pipeline and wells. This data were derived from flying height of 400m above the ground. The deepest slice (Fig. 6) at depth of 4740m produced anomaly which corresponded to basement rock. The intermediate depths in the power spectrum may represent the volcanic rocks (1400m and 2525m) in Fig. 6.

***Total Horizontal gradient technique*:** Through the use of the Geosoft software, the total horizontal gradient method was applied to locate density boundaries of gravity data or susceptibility boundaries of magnetic (as Pseudogravity) data (Ma *et a*l 2006; Bilim, 2007; Pilkington, 2007). Generally, the horizontal gradient of magnetic anomaly which corresponded to a tabular body tends to overlie the edges of the body if the edges were vertical and isolated from each other (Cordell, 1979; Cordell and Grauch, 1985). These authors discussed a technique to estimate the location of abrupt lateral changes in magnetization or mass density of upper crest rocks. The main advantage of the horizontal gradient method was that it was least susceptible to noise in the data, because it only required the calculations of the two first-order horizontal derivatives of the field (Phillips, 1998). This method was also robust in delineating both shallow and deep sources, in comparison with the vertical gradient method, which was useful only in identifying shallower structures. The amplitude of the horizontal gradient (Cordell and Grauch, 1985) is expressed as:

$$HG_g = \sqrt{\left(\frac{\partial g}{\partial x}\right)^2 + \left(\frac{\partial g}{\partial y}\right)^2}$$

Where ($\partial g/\partial x$) and ($\partial g/\partial y$) are the horizontal derivatives of the magnetic data. This method is normally applied to grid data rather than profiles. Maximum magnitudes of horizontal magnetic gradient anomaly occur above geological

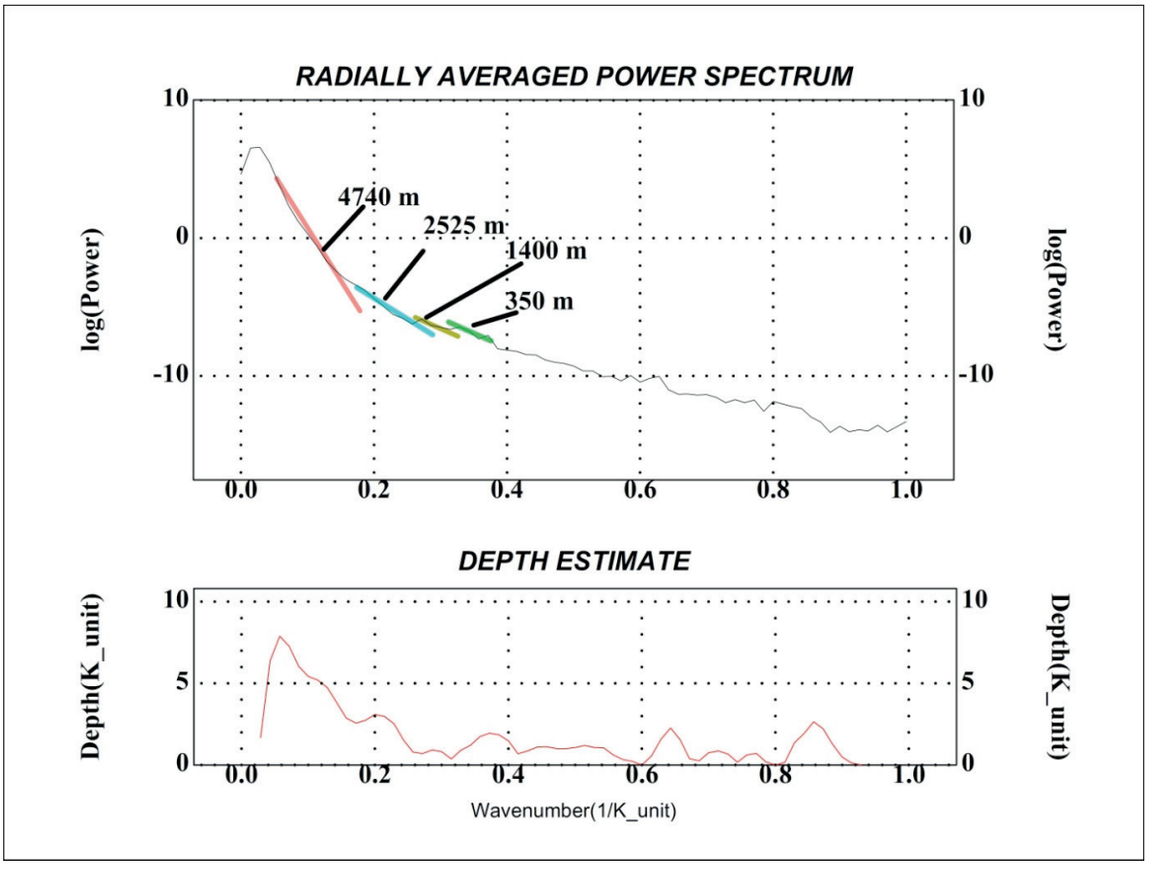

Fig. 6 Power spectrum result of study area.

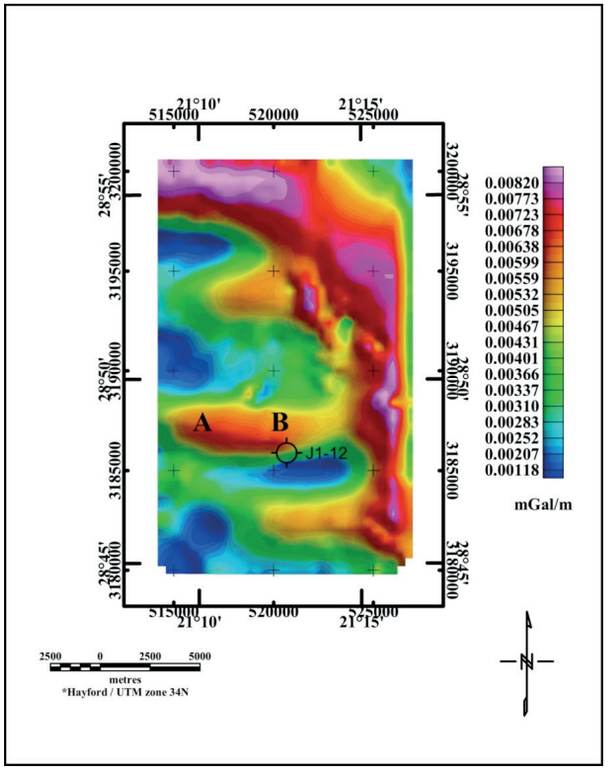

Fig. 7 Total horizontal derivative of total magnetic intensity (TMI) in the study area. The high gradient areas indicated by A and B.

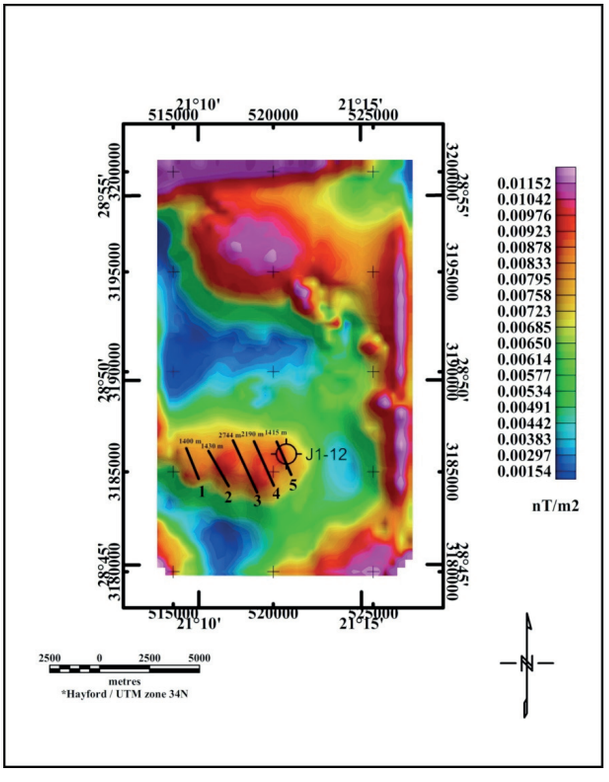

Fig. 8. Analytic signal of magnetic data of Farigh area. Lines 1–5 are the selected profiles that were used to estimate the depths from the analytic signal.

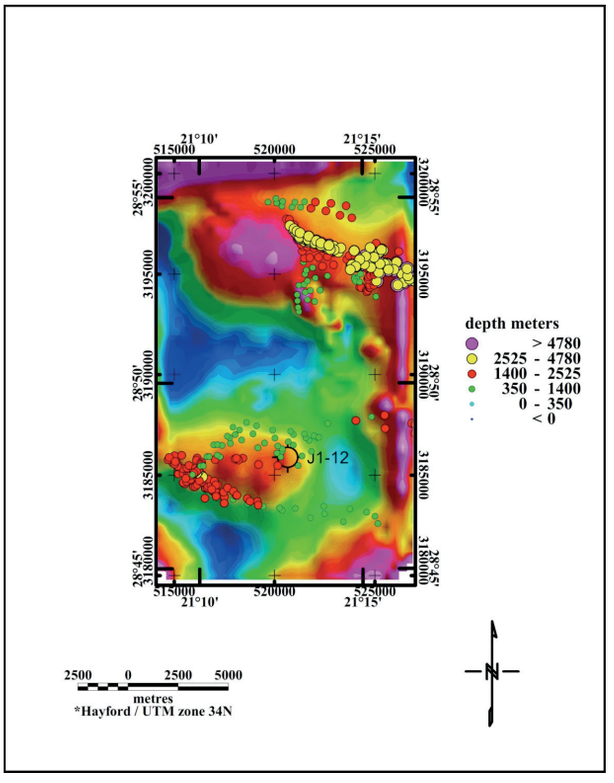

Fig. 9 3D Euler deconvolution for magnetic intensity anomaly over Farigh area. Circles indicate the depths of anomalies representing faults patterns, throws and their depths in the geological formations.

boundaries such as faults or steeply dipping lithological boundaries. Areas of steep lateral gradient have higher scalar amplitude values of horizontal magnetic gradient (Blaky and Simpson, 1986). However Fig. 7 shows the horizontal-gradient map of the study area. The magnetic field was transformed into a Pseudogravity field using an I= 41.579° and D= 2.322° . From the Pseudogravity field, the magnitude of horizontal gradient was calculated by using Geosoft software. High gradient values indicated as A and B (Fig. 7) were observed at locations that may be interpreted as the igneous bodies of the study area. The directions of the bodies were estimated in E-W direction.

***Analytic Signal Method*:** The basic concepts of the analytic signal method using 2D magnetic data were extensively discussed by Nabighian (1972, 1974, 1984) and Green and Stanley (1975). Roest *et al* (1992) showed that the amplitude (absolute value) of the 3D analytic signal at location *(x, y)* can be easily derived from the three orthogonal gradients of the total magnetic field. In the analytic signal method, it is assumed that the causative sources are magnetic contacts. The depth was estimated using the width of the analytic signal anomalies between inflection points (MacLeod *et al* 1993). The analytic signal signature of the Farigh area was calculated (Fig. 8) in the frequency domain using the fast Fourier transform technique (Geosoft, 2009). Higher values of the analytic signal are observed mainly in some regions of the study area (Fig. 8), indicating that these regions have significant susceptibility contrasts that produce identifiable signatures on the map. To estimate the depth of the contacts from the analytic signal, we selected five profiles over the regions where contrasts could be found. The depth values for profiles 1, 2, 3, 4, 5 respectively 1400m,1430m, 2744m, 2190m and 1415m. The depth from well J1-12 is 1400m matched to the depth results from profile 5 (1415m).

***Euler deconvolution technique*:** The Euler deconvolution technique is commonly used to estimate depth and location of the magnetic-gravity source anomalies. Euler deconvolution has come into wide use for automatic estimates of field source location and depth (Bournas *et al* 2003; Shepherd *et al* 2006; Chennouf *et al* 2007; Li *et al* 2008). This method was established by Thompson (1982) and has been applied essentially to real magnetic data along profiles. Reid *et al* (1990) followed up a suggestion in Thompson's paper and developed the equivalent method, which operates on gridded magnetic data. The application of Euler deconvolution to magnetic data has been carried out by several authors such as Wilsher (1987), Corner and Wilsher (1989), Klingele *et al* (1991), Marson and Klingele (1993), Fairhead *et al* (1994) and Huang *et al* (1995).

The 3-D equation of Euler deconvolution given by Reid *et al* (1990) is:

$$(x-x_o)\frac{\partial g}{\partial x}+(y-y_o)\frac{\partial g}{\partial y}+(z-z_o)\frac{\partial g}{\partial z}=\eta(\beta-g) \quad (1)$$

Equation (1) can be rewritten as:

$$x\frac{\partial g}{\partial x}+y\frac{\partial g}{\partial y}+z\frac{\partial g}{\partial z}+\mathrm{h}\,g=x_o\frac{\partial g}{\partial x}+y_o\frac{\partial g}{\partial y}+z_o\frac{\partial g}{\partial z}+\mathrm{h}\,\mathrm{b} \quad (2)$$

Where g is the magnetic or gravity anomaly detected at(x,y,z) due to a body located at (x_0,y_0,z_0). b refers to the regional field at (x,y) and h is a constant defined as " structural index" (SI), different for various geological structures. For example, in the magnetic case, SI = 3 for a sphere, SI = 2 for a

horizontal cylinder and pipes, SI = 1 for a sills and dykes, SI = 0.5 for thick step, SI = 0.0 for geological contacts and faults (Reid *et al* (1990, 2003).

Results of the Euler deconvolution of re-gidding magnetic data (400m, high resolution) in the study area (Farigh area) using a moving windows size of 10 (4km x 4km), and an SI=0.5 are shown in Figure 11. The interpretation of Euler solutions indicates that the NW-SE anomalies were truncated by NE-SW trends and characterized the whole structural setting or faults of the Farigh area. The depth of fault contacts ranged from power spectrum applied to Euler depth were 350m, 2525 m, 1400 m and 4740 m respectively. These contacts were interpreted as contacts plotted and statistically analyzed (Fig. 9). The depth levels of 1400m and 2525m (Fig. 9) were chosen to cover structural boundaries in the top of igneous bodies (especially Nubian sandstone) indicated that the depth from borehole penetrated the igneous bodies (J1-12) were matched with the results of Euler deconvolution in the study area.

DISCUSSION AND CONCLUSIONS

Total magnetic derivative results compare very well with the 3D Euler Deconvolution and tectonic elements in the study area. High magnetic gradient values delineate NW-SE and E-W fault trends which mark the faulted eastern and southern part of Sirt basin, respectively. Estimated depth of igneous body in the study area is from analytic signal. The depth values for profiles 1,2,3,4,5 respectively 1400m,1430m, 2744m,2190m and 1415m.The 3D Euler deconvolution applied to the total magnetic intensity data using structural index SI=0.5 and window size W=10 is from 350 m to 1400 m represents solutions in the shallow parts of study area. Depth of 1400 m to 2525 m is critically indicative of intermediate depth. Deeper solution at depth of 4740 m below the surface was interpreted as basement rocks. The depth 1400m from well J1-12 matched to the depth results from power spectrum in the second slop (1400m), however, the depth from analytic signal profile 5 (1415m) matched the depth from J1-12 and finally depth 1400m to 2525m from 3D Euler deconvolution using SI=0.5,W=10 also matched the depth in the J1-12.

ACKNOWLEDGMENTS

We would like to thank the National Oil Corporation of Libya and the Libyan Petroleum Institute for giving the permission to publish the present data. We would also like to thank Dr A.B. Reid for his advice on the use of Euler deconvolution.

REFERENCES

Abadi, A.M. (2002). Tectonics of the Sirt Basin: Inferences from Tectonic Subsidence Analysis, Stress Inversion, and Gravity Modeling. PhD Thesis Vrije Universiteit, Amsterdam, Netherlands.

Ahlbrandt, T. S. (2001). The Sirte Basin Province of Libya: Sirte-Zelten Total Petroleum System. *U.S. Geological Survey Bulletin,* 2202-F (Version 1.0).

Bilim, F. (2007). Investigations into the tectonic lineaments and thermal structure of Kutahya-Denizli region, western Anatolia, from using aeromagnetic, gravity and seismological data. *Physics of the Earth and Planetary Interiors*, 165 (3-4):135-146.

Blakely, R. .J. and Simpson, R. W. (1986). Locating edges of source bodies from magnetic and gravity anomalies. *Geophysics*, 51 (7): 1494-1498.

Bournas, N., Galdeano, A., Hamoudi, M. and Baker, H. (2003). Interpretation of the
aeromagnetic map of Eastern Hoggar (Algeria) using the Euler deconvolution, analytic signal and local wavenumber methods. *Journal of African Earth Sciences*, 37 (3-4): 191-205.

Chennouf, T., Khattach, D., Milhi, A., Andrieux, P. and Keating, P. (2007). Major structural trends in northeastern Morocco: The contribution of gravimetry. *Comptes Rendus–Geoscience*, 339: 383-395.

Cordell, L. (1979). Gravimetric expression of graben faulting in Santa Fe Country and the Espanola Basin, New Mexico, *Guidebook to the 30th Field Conference*, Santa Fe Country, New Mexico Geological Society (Ed), *New Mexico Geological Society, Socorro*: 59-64.

Cordell, L. and Grauch, V. J. S. (1985). Mapping basement magnetization zones from aeromagnetic data in the San Juan Basin, New Mexico. In: W. J. Hinze (Ed). The utility of regional gravity and magnetic anomaly maps: *Society of Exploration Geophysicists*: 181-197.

Corner, B. and Wilsher, W. A. (1989). Structure of the Witwatersrand basin derived from interpretation of the aeromagnetic and gravity data. In: G. D. Garlan, (Ed). Proceedings of exploration ’87, third decennial international conference on geophysical and geochemical exploration for

minerals and groundwater. *Ontario Geological Survey, Special, **3***: 532-546.

El-Hawat, A. S., Missallati, A. A., Bezan, A. M and Taleb, M. T, (1996). The Nubian Sandstone in Sirt Basin and its Correlatives. In: M. J. Salem, A. S. El-Hawat and A. M. Sbeta (Eds), *The Geology of Sirt Basin*. Elsevier, Amsterdam: 3-30.

Fairhead, J. D., Bennet, K. J., Gordon, R. H. and Huang, D. (1994). Euler: Beyond the Black Box. *64th Annual International Meeting, Society of Exploration Geophysicists*, Expanded Abstracts: 422-424.

Geosoft, Reference Manual (2009). Software for Earth Sciences Geosoft INC., Toronto, Canada.

Goudarzi, G. H. (1980). Structure-Libya. In: M. J. Salem and M. T. Buserwil, (eds.). *The Geology of Libya*. ***vol. 3***: 879-892.

Gras, R. and Thusu, B. (1998)**.** Trap architecture of the Early Cretaceous Sarir Sandstone in the eastern Sirt Basin. In: D. S. Macgreor, R.T. J. Moody and D. D. Clark-Lowes (eds), Petroleum Geology of North Africa. *Geological Society, London, Special Publication NO.* 132: 317-334.

Guiraud, R. and Bosworth, W. (1997). Senonian basin inversion and rejuvenation of rifting in

Africa and Arabia: synthesis and implications for plate scales tectonics. *Tectonophysics,* 282: 39-82.

Hallet, D. (2002). Petroleum Geology of Libya. Elsevier, Amsterdam: p487.

Huang, D., Gubbins, D., Clark, R. A. and Whaler, K. A., 1995. Combined study of Euler's homogeneity equation for gravity and magnetic field. *57th Conference and Technical Exhibition EAGE, Glasgow*, Extended Abstracts: p144.

Klitzsch, E. (1971). The structural development of part of North Africa since Cambrian time. In: C. Gray (ed.), *First Symposium on the Geology of Libya*. Faculty of Science, University of Libya, Tripoli: 253-262.

Klitzsch, E. H and Squyres, C. H. (1990). Paleozoic and Mesozoic geological history of Northeastern Africa based upon new interpretation of Nubian Strata. *AAPG Bull.*, 74: 1203-1211.

Klingele, E. E., Marson, I. and Kahle, H. G. (1991). Automatic interpretation of gravity gradiometric data in two dimensions: vertical gradient. *Geophysical Prospecting*, 39: 407-434.

Tawadros, E, Rasul, S. M, and Elzaroug, E. (2001). Petrography and palynology of quartzites in the Sirte Basin, central Libya. *Jour. African Earth Sciences*, 32: 373-390.

Van der Meer, F. and Cloetingh, S. (1993). Intraplate stresses and subsidence history of the Sirte Basin (Libya). *Tectonophysics,* 226: 37-58.

Li, C.-F., Zhou, Z., Hao, H., Chen, H., Wang, J., Chen, B. and Wu, J. (2008). Late Mesozoic tectonic structure and evolution along the present-day Northeastern South China Sea continental margin. *Journal of Asian Earth Sciences*, 31 (4-6): 546-561.

Ma, Z.-J., Gao, X.-L. and Song, Z.-F. (2006). Analysis and tectonic interpretation to the horizontal-gradient map calculated from Bouguer gravity data in the China mainland. *Chinese Journal of Geophysics (Acta Geophysica Sinica)*, 49 (1): 106-114.

Marson, I., and Klingele, E. E., (1993). Advantages of using the vertical gradient of gravity for 3-D interpretation. *Geophysics*, 58: 588-1595.

Phillips, J. D. (1998)**.** Processing and interpretation of aeromagnetic data for the Santa Cruz Basin-Patahonia Mountains area, South-Central Arizona. *U. S. Geological Survey Open-File Report*: 02-98.

Pilkington, M. (2007)**.** Locating geologic contacts with magnitude transforms of magnetic data. *Journal of Applied Geophysics*, 63 (2): 80-89.

Reid, A. B., Allsop, J. M., Granser, H., Millet, A. J. and Somerton, I. W. (1990). Magnetic interpretation in three dimensions using Euler Deconvolution. *Geophysics*, 55: 80- 91.

Reid, A. B., Fitz Gerald, D. and McInerney P. (2003). Euler Deconvolution of gravity data. *Society of Exploration Geophysicists (SEG), Annual Meeting*, 2003: 580-583.

Reid, A. B. (2003). Short note: Euler magnetic structural index of a thin-bed fault. *Geophysics*, 68: 1255-1256.

Robertson Group Comp. (1970)**.** Geological study in the concession 12. *Unpblished report*.

Shepherd, T., Bamber, J. L. and Ferraccioli, F. (2006). Subglacial geology in Coats Land, East Antarctica, revealed by airborne magnetics and radar sounding. *Earth and Planetary Science Letters*, 244 (1-2): 323-335.

Thompson, D. T. (1982). EULDPH – A new technique for making computer-assisted depth estimates from magnetic data. *Geophysics*, 47: 31-37.

Wilsher, W. A. (1987). A structural interpretation of the Witwatersrand basin through the application of the automated depth algorithms to both gravity and aeromagnetic data. *Unpublished MSc. Thesis*, University of Witwatersrand.